Corrosion Inhibitive Potentials of Some N-Alkyl Benzimidazoles and their Corresponding Ionic Liquids on a Mild Steel Surface: Experimental and Theoretical Approach

Umar B. Suleiman[1], Umar Yunusa[2], Aminu Muhammad[1] and Mansur B. Ibrahim[*1]

[1]*Department of Pure and Industrial Chemistry, Bayero University, Kano, Nigeria*
[2]*Chemistry Department, King Fahd University of Petroleum and Mineral, Dhahran, 31261, Saudi Arabia*
[*]Corresponding author: mansurbi.chm@buk.edu.ng

Received 20/01/2022; accepted 10/05/2022
https://doi.org/10.4152/pea.2023410504

Abstract
U2 and U4 were successfully synthesized from $C_7H_6N_2$ N-alkylation (general and useful route to quaternary ammonium salts NH4Cl from tertiary amines) with alkyl bromides. The products were further alkylated to the corresponding ILs: U5 and U7. All the synthesized compounds were characterized by spectroscopic techniques, and their compositions were established through elemental analysis. The synthesized compounds were investigated as inhibitors for MS corrosion, using 1 M HCl as a model solution. WL experiments, surface analysis, quantum chemical calculations and MD simulation methods were used for evaluating the inhibitors anticorrosion properties. The results showed that ILs possessed remarkable inhibition properties under the studied conditions. U5 displayed the highest IE of 95.22%, at 200 ppm. ILs corrosion IE(%) was ascribed to their adsorption onto the MS surfaces, which followed the Langmuir's isotherm. SEM revealed the formation of a barrier film by the inhibitors on the MS surface. Finally, the experimental results were corroborated by theoretical quantum chemical calculations and MD simulation studies. The studied inhibitor molecules interaction energies with the Fe surface followed the order U5 > U7 > U2 > U4, which is consistent with the experimental data.

Keywords: corrosion inhibition, ILs, MD simulations, MS, N-alkylbenzimidazoles, quantum chemical calculations and SEM.

Introduction•

Corrosion remains a major obstacle for industries all over the world [1-5]. It is often associated with substantial economic losses, such as reduced efficiency, increased maintenance costs and plants shutdown [3-8].

MS is widely used in industrial applications, transmission pipelines, construction, metal processing equipment, storage tanks, etc. [4]. However, the major drawback

• The abbreviations and symbols definition lists are in pages 376-377.

with this alloy use is its low resistance to corrosion in acidic media [9], since HCl solutions are commonly used for MS pickling, cleaning and acid descaling.
Because of the acidic solutions aggressive attack, inhibitors are commonly employed for safeguarding metals surfaces integrity [8-13]. The development of efficient corrosion inhibitors remains a subject of intense research [14]. Most of the studied inhibitors are organic compounds containing heteroatoms (such as N, P, S and O), polar functional groups, π-electron systems and aromatic rings in their structures [11, 15, 16]. The IE% of organic compounds containing heteroatoms increases in the order of O < N < S < P [15].
The compounds inhibition mechanism is ascribed to their adsorption onto the metal surface, thus forming a protective film that hampers anodic/cathodic reactions on the metal, thereby mitigating the corrosion process [17-22].
There exists a diverse list of organic compounds studied as inhibitors for MS corrosion in 15% HCl solutions. Among them are spiropyrimidinethiones, alcohol-based inhibitors, trans-cinnamaldehyde, cationic-gemini surfactants, S-N Schiff bases and derivatives of $C_7H_6N_2$, pyranopyrazole, imidazole, pyridine, pyrazolone, benzyl quinolinium chloride and amino acids [18, 20].
Recently, the study of a variety of polymers as inhibitors for MS corrosion has become the focus of research, due to their multiple adsorption sites, handiness, cost-effectiveness, safety in handling and environmental friendliness [18-22].
Although there are many protection strategies adopted to control metal substrates corrosion in diverse aggressive media, the use of corrosion inhibitors for internal pipeline rust protection is the most practical and cost-effective method [21].
The key performance indicators for corrosion inhibitors selection include their economic availability, effectiveness to protect the metal substrate, and environmental friendliness [19].
ILs are compounds that have revolutionized research centers and chemical industries in recent years [23-38]. Recently, they have received considerable attention, because of their environmental friendliness and good anti-corrosion activity [27-37].
Due the excellent corrosion inhibition behavior of heteroatomic organic compounds with conjugated π-electron systems and polar groups, N-alkylbenzimidazoles, such as U2 and U4, and their corresponding salts (ILs), namely, U5 and U7, were herein synthesized and characterized.
The corrosion inhibition potential of these compounds was studied by the WL technique. Surface examination to verify ILs adsorption onto MS was achieved using SEM. Theoretical quantum chemical calculations and MD simulations were employed in order to provide atomic and molecular insights on the differences in the IE(%) of the two IL inhibitors, and for further complementing the experimental data.

Experimental

Materials

Materials for U2, U4, U5 and U7 synthesis were purchased from Sigma Aldrich, and used as-received. All solvents were of analytical grade, and were directly used without further purification. The synthesized products were purified either using MC (packed

with 60 F silica gel, from Fluka-Chemie AG, Buchs, Switzerland), or by washing them with the appropriate solvent.

Instrumentation

^{1}H-NMR spectral analyses were carried out in $CDCl_3$ solvent using a Bruker 400 MHz ultra-shield instrument. δ were recorded in ppm, using TMS as reference. J was given in Hz. ^{1}H-NMR signals were labeled as s, d, t and m. FT-IR spectra were recorded using an Agilent technology FT-IR spectrophotometer (Cary 630). Elemental analyses were performed with a Perkin Elmer Series 11 (CHNS/O) 2400 analyzer. Merck 60 F254 silica gel plates (with a layer thickness of 250 μm) were used for TLC analyses. An electro thermal apparatus (Stuart SMP 10) was used for measuring the solid compounds mp. Surface analysis experiments were performed using a SEM (FEI Quanta 450), at an acceleration voltage of 20 kV and x1000 magnification.

$C_7H_6N_2$ derivatives synthesis

U2 and U4 synthesis

$C_7H_6N_2$ (10 mmol, 0.38 g) and the appropriate alkyl bromide (11 mmol) were introduced into a cleaned and dried 250 mL three-necked round bottom flask. KOH and K_2CO_3 (12 mmol both and 1.656 and 0.672 g each, respectively) were added to the flask. The mixture was dissolved in anhydrous CH_3CN (80 mL), and stirred for 24 h, at 80 ºC.

The reaction was monitored using TLC (50% $C_4H_8O_2$ and 50%: C_6H_{14}), until no free $C_7H_6N_2$ was observed. The mixture was cooled down to room T, and CH_3CN was removed by a rotary evaporator. The crude product was extracted with $C_4H_8O_2$ and H_2O. The combined organic layer was dried using anhydrous magnesium sulfate. The solvent was removed using a rotary evaporator, and the crude product was purified using silica-gel MC with $C_4H_8O_2$-C_6H_{14} as eluent, for obtaining pure U4.

U2

Yellow solid with 91.7% yield and 115 ºC mp ^{1}H-NMR (400 MHz, $CDCl_3$) δ (ppm): 5.43 (s, 2H CH_2); 7.38-7.29 (m, 6H, CH aromatic, J = 5.6 Hz); 7.24 (d, 2H, CH aromatic, J = 7.6 Hz); 7.88 (d, H, CH aromatic, J = 8.0 Hz); and 8.25 (s, H, NCHN). FT-IR: 3028 cm^{-1} (C-H), 1490 cm^{-1} (C = N), 1447 cm^{-1} (C = C). Analytic calculations and found values for $C_{14}H_{12}N_2$ were: C = 80.77 and 81.06; H = 5.78 and 5.98; and N = 13.46 and 13.67, respectively (Fig. 1).

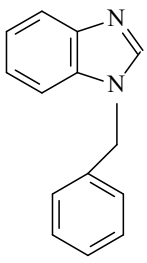

Figure 1. U2.

U4

Thick brown oil with 88.5% yield. ^{1}H NMR (400 MHz, $CDCl_3$) δ (ppm): 0.95 (t, 3H, CH_3, J = 7.2 Hz), 1.41-1.31 (m, 2H, CH_2, J = 7.6 Hz), 1.88-1.82 (m, 2H, CH_2, J = 7.2 Hz), 4.17 (t, 2H, NCH_2, J = 6.8 Hz), 7.83-7.26 (m, 4H, CH aromatic, J = 2.8 Hz) and 7.96 (s, 1H, NCHN). FT-IR: 2979 cm^{-1} (C-H), 1458 cm^{-1} (C=C) and 1480 cm^{-1} (C=N). Analytic calculations and found values for $C_{11}H_{14}N_2$ were: C = 75.86 and 76.02; H = 8.05 and 8.36; and N = 16.09 and 16.37, respectively (Fig. 2).

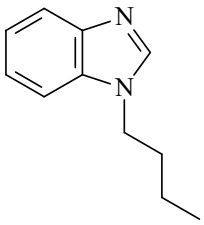

Figure 2. U4.

U5 and U7 synthesis

1-alkylbenzimidazole (2.4 mmol) and benzyl bromide (3 mmol, 0.36 mL) were taken up into a cleaned and oven-dried 25 mL round bottom flask. THF (10 mL) was added. The mixture was refluxed for 14 h, at 70 ºC. After the reaction was completed, the product was cooled and decanted to obtain the crude 1,3-dialkylbenzimidazolium salt, which was then washed several times with diethyl ether. The product was analyzed using TLC (50% $C_4H_8O_2$ and 50% C_6H_{14}), and further washed with ether, until no free 1-alkylbenzimidazole was observed.

U5

White solid with 92.5% yield and 140 ºC mp. ^{1}H NMR (400 MHz, $CDCl_3$) δ (ppm): 1.69 ($CDCL_3$), 5.89 (s, 2H, NCH_2), 7.61-7.28 (m, 14H, CH aromatic, J = 2.8 Hz), 11.62 (s, 1H, NCHN). FT-IR: 2948 cm^{-1} (C-H), 1559 cm^{-1} (C=N), 1458 cm^{-1} (C=C). Analytic calculations and found values for $C_{21}H_{19}N_2Br$ were: C = 66.49 and 66.10; H = 5.01 and 5.15; and N = 7.39 and 7.30, respectively (Fig. 3).

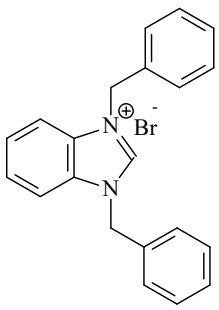

Figure 3. U5.

U7

White solid with 87.9% yield and 158 °C mp. ^{1}H NMR (400 MHz, $CDCl_3$) δ (ppm): 1.10 (t, 3H, CH_3, J = 7.2 Hz), 1.60-1.53 (m, 2H, CH_2, J = 7.6Hz), 1.80 (s, $CDCl_3$), 2.20-2.13 (m, 2H, CH_2, J = 7.6 Hz), 4.70 (t, 2H, NCH_2 aliphatic, J = 7.6 Hz), 5.98 (s, 2H, NCH_2 aromatic), 7.79-7.35 (m, 9H, CH aromatic, J = 8Hz), 11.67 (s, 1H, NCHN). FT-IR: 2951 cm^{-1} (C-H), 1428 cm^{-1} (C=C), 1579 cm^{-1} (C-N). Analytic calculations and found values for $C_{18}H_{21}N_2Br$ were: C = 62.61 and 62.56; H = 6.09 and 6.06; and N = 8.12 and 8.19, respectively (Fig. 4).

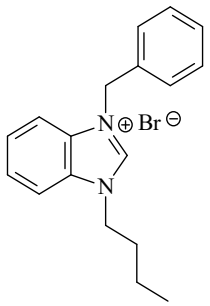

Figure 4. U7.

Corrosion inhibition studies

Samples preparation

MS sample, with the composition (wt%) of C 0.12%, Cu 0.01%, Mn 0.11%, P 0.02%, Si 0.02%, Sn 0.01%, Ni 0.02% and the remaining Fe, was used for the corrosion studies. Test coupons with the dimensions 5.0 × 3 × 0.25 cm were mechanically cut and abraded with different SiC abrasive papers grades (400, 600, 800, 1500 and 2000). Then, they were rinsed with distilled H_2O, degreased in acetone, dried in warm air and stored in a desiccator. The corrosive medium (1 M HCl) was prepared by appropriately diluting 37% analytical grade HCl with distilled H_2O. The studied inhibitors C range was from 50 to 200 ppm, and the used electrolyte volume was 100 mL in all studies.

WL determination

WL measurements were performed at 308 K. Accurately weighed test coupons (treated with 0, 50, 100, 150 and 200 ppm by weight of the appropriate corrosion inhibitors) were immersed in 100 mL 1 M HCl. The pre-determined optimum immersion time of 12 h was uniformly used for the WL study.

After the experiments, the specimens were retrieved from the corrosive solution, thoroughly washed to remove the corrosion products with a SiC abrasive paper, properly rinsed with distilled H_2O, degreased in C_3H_6O, then dried, and finally reweighed. Triplicate experiments were performed for each inhibitor C. The mean WL data were used to compute the C_R (mg/cm^{-2}/h^{-1}) and the inhibitors IE(%), as per Eq 1 and 2.

$$C_R = \frac{W_o - W_i}{St} \quad (1)$$

where S denotes the MS specimen surface area (cm^2); t represents the immersion time (h); W_o and W_i represent the WL (g), before and after immersion in the test solution, respectively;

$$IE_{\%} = \frac{C_R^o - C_R^i}{C_R^o} \times 100 \qquad (2)$$

where C_R^o and C_R^i are MS specimens C_R ($g/cm^{-2}/h^{-1}$) without and with inhibitors, respectively. To determine T dependence on IE%, the experiment was repeated at 35, 45 and 55 ºC, using 200 ppm of the examined inhibitors. T was regulated using a thermostatic H_2O bath.

SME analysis

Surface analysis experiments were performed using a SME (FEI Quanta 450), at an acceleration voltage of 20 Kv, and x1000 magnification.

Before the analysis, the coupons surfaces were appropriately cleaned and carefully dried. The polished samples, including the untreated and the treated ones, were carefully examined.

Theoretical studies

The molecules geometries were optimized using Dmol3 module, at B3LYP/DND level of theory, as implemented in Materials Studio (version 8.0) software.

After optimization, E_{HOMO}, E_{LUMO}, ΔE and other reactivity parameters were calculated.

The interaction between IL molecules and the Fe surface was probed using Forcite module of Materials Studio 8.0 software package.

Before simulations, Fe (1 1 0) plane was first cleaved from Fe crystal, and its surface was then optimized to the minimum energy.

The simulations were conducted in a simulation box (27.8 × 28.7 × 25.3 Å), with periodic boundary conditions, at a time step of 1 fs, using a simulation time of 500 ps, and a COMPASS force-field, under NVT ensemble, at 298 K. After simulations, E_{int} between the inhibitor molecule and the Fe surface was computed using Equation 3.

$$E_{int} = E_{Total} - (E_{surface + solution} + E_{inhibitor}) \qquad (3)$$

where E_{Total} expresses the entire system total potential energy, $E_{surface + solution}$ reflects the energy of Fe (110) and of the blank solution, and $E_{inhibitor}$ represents the isolated inhibitor molecule energy.

Results and discussion

U2 and U4 synthesis

U2 and U4 were successfully synthesized by $C_7H_6N_2$ deprotonation, using KOH/K_2CO_3 as a base, at room T. The deprotonated $C_7H_6N_2$ was sufficiently nucleophilic to attack C_7H_7Br primary C, and generate the corresponding U2.

The reaction time was prolonged and T increased, when necessary, in order to ensure complete alkylation [15].

After the reaction, $C_{14}H_{12}N_2$ (U2) was obtained as a yellowish-brown powder with a high isolated yield (92%). $C_7H_6N_2$ reaction with C_4H_9Br, under identical reaction conditions, produced the corresponding U4, as a thick brown oil, with an isolated yield of 88%. An obvious reason for U2 relatively higher isolated yield than that of U4 is that the former is more reactive towards a nucleophilic attack than the latter [16, 37-40].

The synthesized U2 and U4 purity was preliminarily examined by TLC, and further subjected to MC. The results showed adequate purity for characterization with spectroscopic methods. Some physical properties of the synthesized compounds, such as mp, were measured and found to comply with the literature values [15, 16, 23-26].

^{1}H-NMR spectra of these compounds showed the various protons indifferent chemical environments. In the U2 ^{1}H-NMR spectrum, the protons on the $(C_6H_5CO)_2$ group CH_2 resonated at a downfield of 5.43 ppm, and appeared as s, indicating $C_7H_6N_2$ successful N-alkylation. The signals at δH 7.38-7.29 ppm indicate an aromatic (CH) presence, while the signal at downfield, δH 8.25 ppm, corresponds to the proton on the $C_7H_6N_2$ frame NCHN.

In the U4 ^{1}H-NMR spectrum, the CH_2 group attached to $C_7H_6N_2$ was observed downfield, at δH 4.17 ppm. This was higher than the other CH_2 on positions 2 and 3 of the C_4H_9 group, which was due to the de-shielding effect caused by the $C_7H_6N_2$ frame N atom. The signal at δH 7.96 ppm was assigned to the proton on the NCHN, which appeared as s.

The signal observed at δH 0.95 ppm represents C_4H_9Br group. IR spectra of these compounds showed an absorption band at around 1458-1490 cm^{-1}, which is characteristic of the C = C and C = N vibrations.

The $(C_6H_5CO)_2$ group presence is characterized by the typical absorption pattern of the aliphatic C-H stretching vibration at 2979-3028 cm^{-1}, which further confirmed successful $C_7H_6N_2$ N-alkylation. The elemental analyses results show consistency between experimental and theoretical values.

ILs synthesis

U5 and U7 ILs were obtained at excellent yields (93 and 88%, respectively). ILs ^{1}H-NMR spectra revealed downfield signals at 11.61 and 11.66 ppm, respectively, assigned to the U5 and U7 NCHN acidic protons, respectively. Moreover, the signal appearance at δH 5.89 and 5.98 ppm, as a sharp s, was due to the CH_2 $(C_6H_5CO)_2$ group proton, which further confirmed the formation of the expected U5 and U7 $C_7H_6N_2$ salts.

The m signal for the U5 and U7 CH aromatic protons was observed within the range from 7.61 to 7.79 ppm. The signal observed at δH 1.1 ppm, as t, was assigned to U7 CH_3 group.

The ^{1}H NMR spectral data of both compounds were in entire agreement with published literature [11-16].

Both ILs FT-IR spectra showed absorption bands at 2948, 1559, 1458, 2951, 1579 and 1428 cm^{-1}, corresponding to the C-H stretching vibrations for CH_2 and CH_3, C=N and C=C of the $C_7H_6N_2$ rings, for U5 and U7, respectively.

Synthesized compounds corrosion IE% on a MS surface

WL analysis

The relationship between the corrosion parameters and the tested inhibitors C is displayed in Table 1.

Table 1. Corrosion parameters of MS in 1 M HCl using various $C_7H_6N_2$ compounds (including ILs) as inhibitors, at different C and T values.

C_{inh}	35 ºC		45 ºC		55 ºC	
(ppm)	C_R	IE(%)	C_R	IE(%)	C_R	IE(%)
0	2.20		5.23		8.78	
U5						
50	1.05	52.27	2.32	55.64	3.42	61.04
100	0.69	68.63	1.39	73.42	1.81	79.38
150	0.38	82.72	0.61	88.33	0.70	92.20
200	0.23	89.54	0.38	92.73	0.42	95.22
U7						
50	1.20	45.45	2.54	51.43	3.69	57.97
100	0.78	64.54	1.57	69.98	2.11	75.96
150	0.48	78.18	0.78	85.08	0.91	89.63
200	0.32	85.45	0.54	89.67	0.61	92.36
U2						
50	1.30	40.90	2.67	48.94	3.79	56.83
100	0.84	61.81	1.69	67.68	2.31	73.69
150	0.53	75.90	0.87	83.26	1.11	87.35
200	0.38	82.72	0.64	87.76	0.81	90.77
U4						
50	1.37	37.72	2.79	46.65	3.98	54.67
100	0.92	58.18	1.80	65.58	2.49	71.64
150	0.60	72.72	0.97	81.45	1.29	85.30
200	0.45	79.54	0.76	85.46	0.98	88.83

The presence of all the studied compounds in the test solution caused a drastic decrease in C_R, reflecting an increase in IE%, which occurred with higher inhibitors C values. This observation might be ascribed to the electron donor (N) and aromatic rings abundance at the metal/solution interface [27].

Maximum IE% was observed with the highest C (200 ppm) of the tested inhibitors. IE% was found to depend on the type of employed inhibitor as follows: U5 > U7 > U2 > U4. IE% variation could be linked to the difference in U5 and U7 ILs molecular structural features. Thus, the best IE (95.22%) was exhibited by U5, at 200 ppm.

U5 superior performance is attributed to the greater number of electron-rich centers (aromatic π-electron system) in its structure, which increased its tendency to transfer electrons into the Fe vacant d-orbitals, thus mitigating the corrosion process [5, 6].

Thermodynamic and activation parameters

Thermodynamic and activation parameters play a crucial role in diagnosing the corrosion inhibitive mechanism [33-40].

WL experiments were performed in the T range from 308 to 328 K, using $C_7H_6N_2$ compounds and their corresponding ILs, at various C values.

E_a for MS dissolution in 1 M HCl was obtained using the Arrhenius equation:

$$\log C_R = \frac{-E_a}{2.303RT} + \log A \qquad (4)$$

where R is the molar gas constant (8.314 J/mol^{-} E_a ^{1}/K^{-1}) and A is the Arrhenius pre-exponential factor.

Fig. 5 illustrates the Arrhenius plot of log C_R against 1/T, for MS corrosion control in a 1 M HCl solution by various inhibitors, at C values ranging from 0 to 200 ppm.

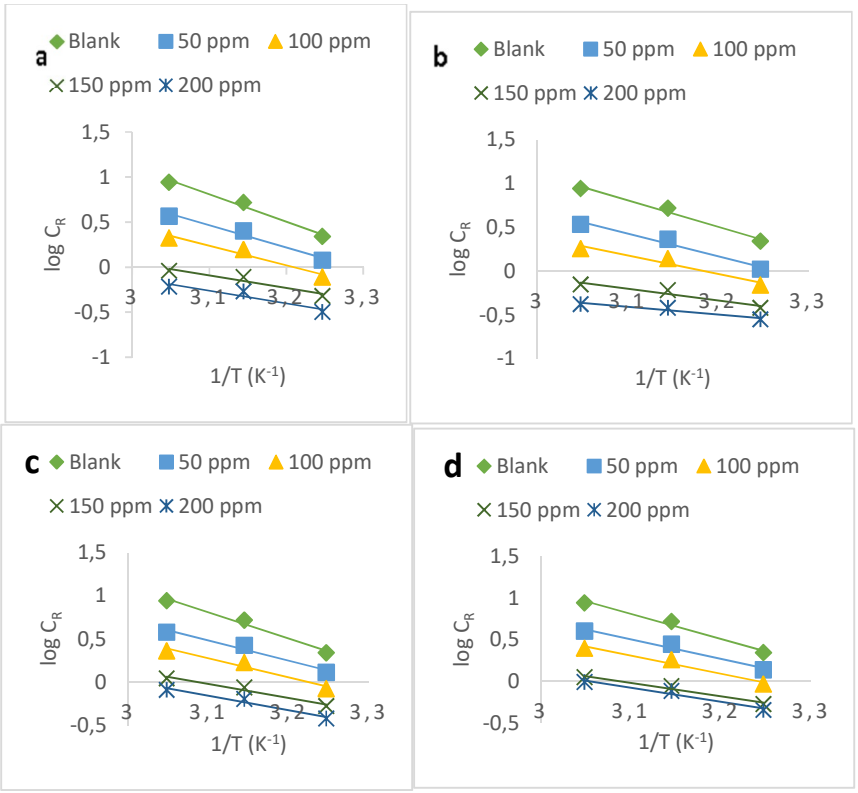

Figure 5. Arrhenius plots of log C_R versus 1/T for MS corrosion inhibition in 1 M HCl by: **(a)** U5, **(b)** U7, **(c)** U2 and **(d)** U4.

E_a values were estimated from the straight lines gradients in Fig. 5, which are shown in Table 2. It is clear from the table that E_a values for the uninhibited solutions were higher than those for the inhibited ones, which indicates a chemisorption process [7]. The energetic barrier was lower, facilitating the formation of Fe^{2+} ions that interacted with the examined inhibitors, forming a protective film at the MS surface.

Adsorption isotherm

The adsorption isotherm provides crucial information on the interaction between the inhibitors and the MS surface.

Several commonly used adsorption isotherms include Langmuir's, Temkin's and Frumkin's, which have been employed for elucidating ILs adsorption behavior onto the MS surface.

Langmuir's adsorption isotherm presented the best fit to the experimental data, as defined by the following equation:

$$\frac{C}{\Theta} = \frac{1}{K_{ads}} + C \qquad (5)$$

The plots of C/Θ against C (Fig. 6), obtained at varying T values, yielded straight lines ($R^2 > 0.99$), affirming the Langmuir's isotherm validity.

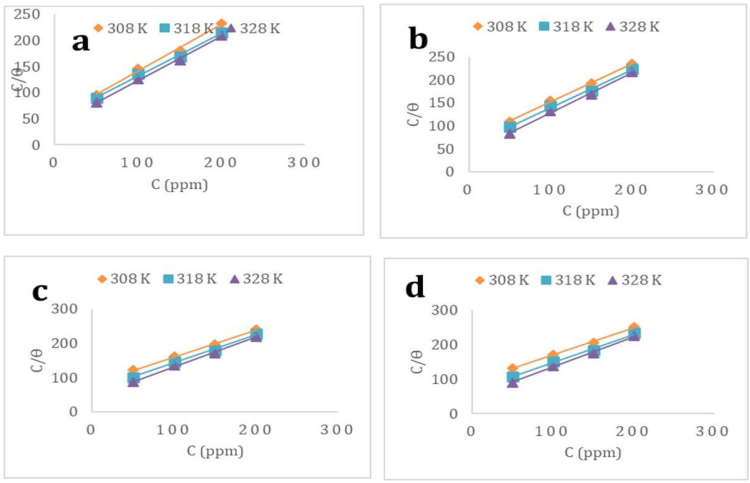

Figure 6. Langmuir plots for: **(a)** U5, **(b)** U7, **(c)** U2 and **(d)** U4.

ΔG^o_{ads} is a key thermodynamic parameter that is linked to K_{ads}, based on the following equation:

$$\Delta G^0_{ads} = -RT \ln(55.5\ K_{ads}) \qquad (6)$$

The constant value of 55.5 represents the H_2O molar C in the solution.

The extracted thermodynamic parameters are collected in Table 2.

Table 2. Activation and thermodynamic parameters for MS corrosion in 1 M HCl without and with inhibitors.

Inhibitor	E_a (Kj/mol^{-1})	A	K_{ads*}(x 10^3)	-ΔG^o_{ads} (kJ/mol^{-1})		
				308 K	318 K	328 K
Blank	57.98	1.6 x 10^{10}				
U5	25.72	9.2 x 10^3	5.18	32.18	33.23	34.27
U7	27.13	1.3 x 10^4	4.45	31.79	32.83	33.86
U2	31.85	2.0 x 10^4	4.04	31.54	32.57	33.59
U4	32.52	1.2 x 10^5	3.77	31.37	32.39	33.40

K_{ads} high values obtained for all the four studied inhibitors signify strong adsorption and, hence, better corrosion inhibition behavior. [8].
It is obvious from Table 2 that ΔG^{o}_{ads} calculated values are negative, which means that the ILs were spontaneously adsorbed onto the metal surface.
In general, ΔG^{o}_{ads} values up to -20 kJ/mol^{-1} are consistent with electrostatic interactions between the inhibitors charged molecules and the charged metallic surfaces (physisorption).
In its turn, ΔG^{o}_{ads} values above -40 kJ/mol^{-1} involve charge transfer or sharing from the inhibitor molecules to the metal surface vacant d-orbitals, to form a coordinate covalent bond (chemical adsorption) [9]. ΔG^{o}_{ads} values in our study ranged from -31.27 to -34.27 kJ mol^{-1}, which suggests the mixed physicochemical adsorption of these molecules onto the MS surface.

Quantum chemical calculations
In order to ascertain the molecular structure influence on IE%, quantum chemical calculations were performed using the B3LYP/DND level of theory. LUMO and HOMO optimized molecular structures and electron density distributions are displayed in Fig. 7.

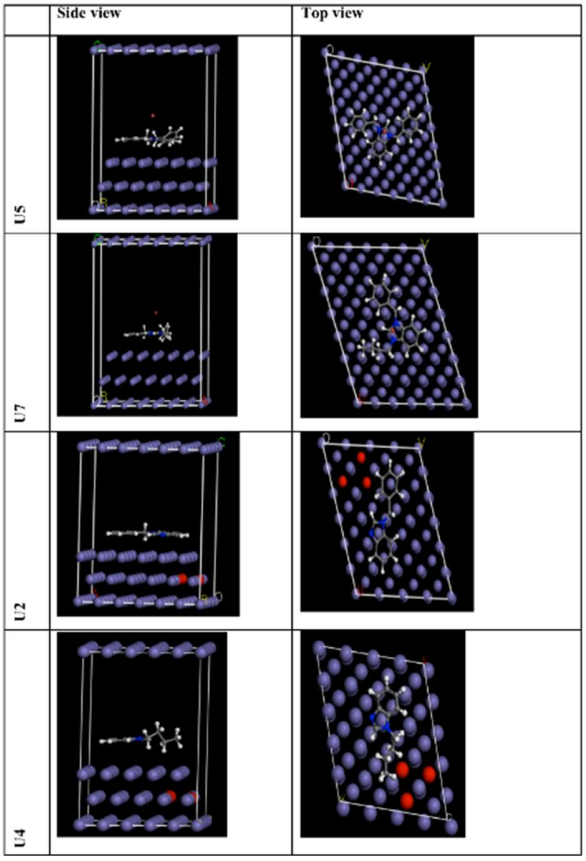

Figure 7. Snapshots of U5, U7, U2 and U4 inhibitors over the Fe (110) surface.

E_{HOMO} and E_{LUMO} are important parameters for the prediction of the chemical species reactivity. E_{HOMO} is often linked to the electron donating ability of a molecule. Thus, its high values mean that a molecule has a high tendency to donate electrons to suitable acceptor molecules with low energy empty molecular orbitals. Conversely, E_{LUMO} low values indicate that the molecule readily accepts electrons from the donor molecules [10]. It is generally accepted that ΔE low values cause better inhibition performance. Quantum chemical parameters, such as E_{HOMO}, E_{LUMO}, ΔE, absolute χ, global η and σ, were calculated, and are summarized in Table 3.

Table 3. Quantum chemical parameters (eV) for the studied inhibitors.

Inhibitor	E_{HOMO}	E_{LUMO}	ΔE	η	σ	χ
U5	-4.85	-2.87	1.98	0.99	1.01	3.86
U7	-4.69	-2.56	2.13	1.07	0.93	3.63
U2	-4.43	-2.19	2.24	1.12	0.89	3.31
U4	-2.22	-1.83	2.39	1.20	0.83	3.04

For the quantum chemical parameters calculations, the following equations were used:

$$\chi = \frac{I+A}{2} = -\frac{E_{HOMO}+E_{LUMO}}{2} \quad (7)$$

$$\acute{\eta} = \frac{I-A}{2} = \frac{E_{LUMO}-E_{HOMO}}{2} = \frac{1}{2}\Delta E \quad (8)$$

η inverse is σ, as follows:

$$\sigma = \frac{1}{\acute{\eta}} \quad (9)$$

According to the results displayed in Table 3, U5 presented E_{HOMO} highest value (-4.85 eV), which shows that it was more easily adsorbed onto the MS surface than U7, U2 and U4. In addition, U5 had ΔE lowest (1.98 eV) and σ highest values (1.01 eV). It is obvious from Table 3 that the ability to donate electrons to the MS surface follows the order: U5>U7>U2>U4, which is in good agreement with these inhibitors IE% experimental order.

MD simulations

MD simulations have been conducted to better understand the interaction between the ILs and Fe (1 1 0) surface. The investigated inhibitor molecules optimized equilibrium configurations (both top and side views) are displayed in Fig. 7, and the calculated energies are shown in Table 4.

By inspecting the shown results, it can be seen that the inhibitor molecules approached the target surface in a nearly flat orientation. Actually, the flat orientation maximized the contact area between the inhibitor molecule and the Fe substrate, creating an obstruction between the latter and the aggressive particles, thus protecting it from corrosion. Meanwhile, the adsorption degree of an inhibitor molecule onto the metal substrate may be predicted using the interaction and binding energies. Higher interaction energies basically show the inhibitor molecule better adsorption onto the

metal surface. Interestingly, the data presented in Table 4 reveal that the simulation system interaction energy value was large and negative, implying that ILs adsorption onto the Fe (1 1 0) surface was strong and spontaneous.

Table 4. Energetic outputs (kcal/mol^{-1}) obtained from the inhibitor molecules MD simulations over the Fe (110) surface.

Inhibitor	Total energy	Molecule energy	Interaction energy
U5	−154.03	−52.09	−101.94
U7	−139.97	−46.77	−93.20
U2	−129.84	−42.55	−87.29
U4	−122.84	−39.55	−83.29

Morphology analysis

SEM micrographs displaying the abraded, corroded and inhibited MS surfaces are presented in Fig. 8 (a). After immersion in the blank 1 M HCl solution, for 12 h, the MS surface was damaged, as it can be seen in Fig. 8 (b). The specimen corroded layer was rather rough and cracked, due to the HCl solution destructive attack. In contrast, the MS specimen with the inhibitors addition exhibited a smooth surface (Fig. 8 (c-d)), which could be attributed to the active centers blocking by the inhibitor molecules on the metal surface. These observations confirm that ILs inhibitive action was based on the formation of a protective film at the MS surface, which protected it against HCl.

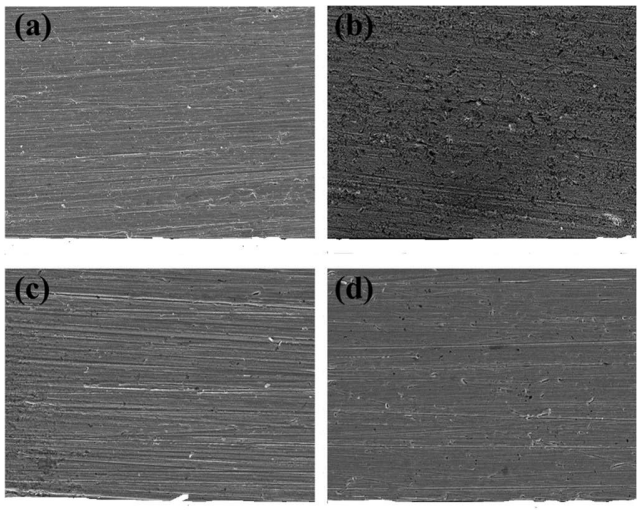

Figure 8. SEM images of the MS surfaces after: **(a)** mechanical abrasion; and immersion in a 1 M HCl solution **(b)** without inhibitor, **(c)** with 200 ppm U5 and **(d)** with 200 ppm U7, at 35 ºC.

Conclusions

The synthesis of U2, U4, U5 and U7 was achieved. The alkyl imidazoles and ILs were found to exhibit good IE(%) of MS corrosion in a 1 M HCl solution. The inhibitors performances were better with higher C values and increased T. U5 and U7 ILs were

found to be better corrosion inhibitors than U2 and U4, with the overall IE(%) increase in the following order: U5>U7>U2>U4. The results obtained from Langmuir's adsorption isotherm and SEM revealed that the inhibitive action mainly occurred through the adsorption process. The theoretical results are in conformity with the experimental findings.

Authors' contributions

Umar B. Suleiman: carried out the synthesis of U2, U4, U5 and U7; carried out physical analyses of the corrosion inhibitors; wrote the corrosion inhibitors synthesis and characterization section. **Umar Yunusa**: carried out the theoretical calculations; carried out the corrosion inhibition analysis; wrote the corrosion inhibitors section and part of their characterization. **Aminu Muhammad**: carried out spectral analyses for $C_7H_6N_2$ salts and ILs and analyzed them; was involved in the drafting, reviewing, and editing of the manuscript. **Mansur B. Ibrahim**: designed the synthesis and carried out the spectral analyses of $C_7H_6N_2$ compounds and ILs; was involved in the drafting, reviewing, and editing of the manuscript.

Abbreviations

^{1}H-NMR: proton nuclear magnetic resonance
A: Arrhenius pre-exponential factor
bp: boiling point
C: concentration
$C_4H_8O_2$: ethyl acetate
C_4H_9: butyl
C_4H_9Br: n-butyl bromide
$(C_6H_5CO)_2$: benzyl
C_6H_{14}: n-hexane
$C_7H_6N_2$: benzimidazolium
C_7H_7Br: benzyl bromide
$CDCl_3$: deuterated chloroform
CH_2: methylene carbon
CH_3: methyl
CH_3CN: acetonitrile
C_R: corrosion rate
d: doublet
E_a: activation energy
E_{HOMO}: energy of the highest occupied molecular orbital
E_{in}: interaction energy
E_{LUMO}: energy of the lowest unoccupied molecular orbital
fs: femtosecond
FTIR: Fourier-transform infrared spectroscopy
HCl: hydrochloric acid
HOMO: highest occupied molecular orbital
IE(%): inhibition efficiency
ILs: ionic liquids:

J: coupling constant
K_2CO_3: potassium carbonate
K_{ads}: adsorption equilibrium constant
KOH: potassium hydroxide
LUMO: lowest unoccupied molecular orbital
m: multiplet
MC: microcolumn chromatography
MD: molecular dynamics
mp: melting points
MS: mild steel
NVT: canonical ensemble, i.e. a collection of all systems of which thermodynamic state is characterized by a fixed number of atoms (N) a fixed volume (V) and a fixed temperature (T)
ppm: parts per million
ps: psicosecond
R^2: determination coefficient
s: singlet
SEM: scanning electronic microscopy
SiC: silicon carbide
T: temperature
t: triplet
THF: tetrahydrofuran
TLC: thin layer chromatography
TMS: tetramethylsilane
U2: $C_{14}H_{12}N_2$ (1-benzylbenzimidazole, i.e. alkylbenzimidazole)
U4: $C_{11}H_{14}N_2$ (1-butylbenzimidazole, i.e. alkylbenzimidazole)
U5: $C_{21}H_{19}N_2Br$ (1,3-dibenzylbenzimidazolium bromide, i.e. dialkylbenzimidazole)
U7: $C_{18}H_{21}N_2Br$ (1-benzyl-3-butylbenzimidazolium bromide, i.e. dialkylbenzimidazole)
WL: weight loss

Symbols definition

δ: chemical shifts
ΔE: energy gap (= E_{LUMO} - E_{HOMO})
ΔG^{o}_{ads}: adsorption energy
η: hardness
θ: surface coverage
σ: softness
χ: electronegativity

References

1. Berisha A, Podvorica F, Mehmeti V et al. Theoretical and experimental studies of the corrosion behavior of some thiazole derivatives toward mild steel in sulfuric acid media. Maced J Chem. Chem. Eng. 2015;34:287-294. http://dx.doi.org/10.20450/mjcce.2015.576
2. Balan P, Shelton MJ, Ching Dol, et al. Modified Silane Films for Corrosion Protection of Mild Steel. Procedia Mater Sci. 2014;6:244-248. https://doi.org/10.1016/j.mspro.2014.07.030

3. Daoud D, Douadi T, Issaadi S et al. Adsorption and corrosion inhibition of new synthesized thiophene Schiff base on mild steel X52 in HCl and H2SO4 solutions.Corros. Sci.2014;79:50-58. https://doi.10.1016/jcorsci.2013.10.025
4. Migahed M, Azzam E, Al-Sabagh A et al. Corrosion inhibition of mild steel in 1 M sulfuric acid solution using anionic surfactant. Mater Chem Phys. 2004;85:273-279. https://doi.org/10.1016/j.matchemphys.2003.12.027
5. Fouda AS, Ellithy AS. Inhibition effect of 4-phenylthiazole derivatives on corrosion of 304L stainless steel in HCl solution. Corros Sci. 2009;51:868-875. https://doi.org/10.1016/j.corsci.2009.01.011
6. Khadraoui A, Khelifa A, Hamitouche H et al. Inhibitive effect by extract of Mentharotundifolia leaves on the corrosion of steel in 1 M HCl solution. Res Chem Intermed. 2014;40:961-972. https://doi.org/10.1007/s11164-012-1014-y
7. Sivakumar V, Velumani K, Rameshkumar S. Colocid dye a potential corrosion inhibitor for the corrosion of mild steel in acid media. Mat Res. 2018;21:4. https://doi.org/10.1590/1980-5373-MR-2017-0167
8. Obot IB, Madhankumar A, Umoren SA et al. Surface protection of mild steel using benzimidazole derivatives: experimental and theoretical approach. J Adhes Sci Technol. 2015;29(19):2130-2152. https://doi.org/10.1080/01694243.2015.1058544
9. Chugh B, Singh AK, Thakur S et al. Comparative Investigation of Corrosion-Mitigating Behavior of Thiadiazole-derived Bis-Schiff bases for Mild Steel in Acid Medium: Experimental, Theoretical, and Surface Study. ACSOmega. 2020;5: 13503-13520. https://dx.doi.org/10.1021/acsomega.9b04274
10. Ebenso E, ArslanT, Kandemirli F et al. Quantum chemical studies of some rhodanineazosulpha drugs as corrosion inhibitors for mild steel in acidic medium. Int J Quantum Chem. 2010;110:1003-1018. https://doi.org/10.1002/qua.22249
11. Fouda AS, Ismail MA, Abousalemet AS et al. Experimental and theoretical studies on corrosion inhibition of 4-amidinophenyl-2,20-bifuran and its analogues in acidic media. RSC Adv. 2017;7:46414. https://doi.org/10.1039/C7RA08092A
12. Dehri I, Ozcan M. The effect of temperature on the corrosion of mild steel in acidic media in the presence of some sulphur containing organic compounds. Mater Chem Phys. 2006;98:316-323. https://doi.org/10.1016/j.matchemphys.2005.09.020
13. Gerengi H, Sahin HI. Schinopsislorentzii extract as a green corrosion inhibitor for low carbon steel in 1 M HCl solution. Ind Eng Chem Res. 2012;51:780-787. https://doi.org/10.1021/ie201776q
14. Goulart CM, Esteves-Souza A, Martinez-Huitle CA et al. Experimental and theoretical evaluation of semicarbazones and thiosemicarbazones as organic corrosion inhibitors. Corros Sci. 2013;67:281-91. https://dx.doi.org/10.1016/j.corsci.2012.10.029
15. Akkoç S, Kayser V, İlhan İÖ et al. New compounds based on a benzimidazole nucleus: synthesis, characterization and cytotoxic activity against breast and colon cancer cell lines. J Organomet Chem. 2017;839:98-107. https://doi.org/10.1016/j.jorganchem.2017.03.037
16. Huynh HV, Mansur BI, et al. Postmodification approach to charge-tagged 1,2,4-Triazole-Derived NHC Palladium(II) complexes and their applications. ACS Organomet. 2017;36:2345-2353. https://doi.org/10.1021/acs.organomet7b00329

17. Shamsuddeen AH, Saviour AU, Shaikh AA et al. Synthesis and Characterization of Cyclic Cationic Polymer and its Anti-corrosion Property for Low Carbon Steel in 15% HCl Solution. Int J Electrochem Sci. 2017;12:9061-9083. https://doi.org/10.20964/2017.10.57
18. Shamsuddeen AH, Saviour AU, Shaikh AA et al. Synthesis, characterization and electrochemical evaluation of anticorrosion property of a tetra polymer for carbon steel in strong acid media. Chin J Chem Eng. 2019;27:965-9.
19. Haladu SA, Umoren SA, Ali SA et al. synthesis and characterization of cyclic cationic polymer and its anti-corrosion property for low carbon steel in 15% HCl solution. Int J Electrochem Sci. 2017;12: 9061-9083. https://doi.org/20964/2017.10.57
20. Umoren SA. Polypropylene glycol: A novel corrosion inhibitor for ×60 pipeline steel in 15% HCl solution. J Mol Liq. 2016;219:946-958. https://doi.org/10.1016/jmolliq.2016.03.077
21. Biswas A, Pal S, Udayabhanu G. Experimental and theoretical studies of xanthan gum and its graft co-polymer as corrosion inhibitor for mild steel in 15% HCl. Appl Surf Sci. 2015;353:173-183. https://doi.org/10.1016/j.apsusc.2015.06.128
22. Aktaş A, Akkoç S, Gök Y et al. Palladium catalyzed Mizoroki-Heck and Suzuki-Miyaura reactions using naphthalenomethyl-substituted imidazolidin-2-ylidene ligands in aqueous media. J Coord Chem. 2013;66(16):2901-2909. https://doi.org/10.1080/00958972.2013.819092
23. Doğan Ö, Demir S, Özdemir I et al. Palladium(II)-NHC complexes containing benzimidazole ligand as a catalyst for C-N bond formation. App Organomet Chem. 2011;25(3):163-167. https://doi.org/10.1002/aoc.1731
24. Gök Y, Akkoç S, Akkurt M et al. Imidazole, pyrimidine and diazepine containing heteroaryl-substituted heterocyclic salts as efficient ligand precursors for Mizoroki-Heck coupling reaction: Synthesis, structural characterization and catalytic activities. J Iran Chem Soc. 2014;11(6):1767-1774. https://doi.org/10.1007/s13738-014-0449-z
25. Ibrahim MB, Suleiman R, Fettouhi M et al. A palladium-bisoxazoline supported catalyst for selective synthesis of aryl esters and aryl amides: Via carbonylative coupling reactions. RSC Adv. 2016;6(82):78826-78837. https://doi.org/10.1039/c6ra15506e
26. Shariati A, Gutkowski K, Peters CJ et al. Comparison of the phase behavior of some selected binary systems with ionic liquids. AIChE J. 2005;(51):1532-1540. https://doi.org/10.1002/aic.10384
27. Zhao H, Xia S, Ma P et al. Use of ionic liquids as green solvents for extractions. J Chem Technol Biotechnol. 2005;80:1089-1096. https://doi.org/10.1002/jctb.1333
28. Kabo GJ, Blokhin AV, Paulechka A et al. Thermodynamic properties of 1-butyl-3-methylimidazolium hexafluorophosphate in the condensed state. J Chem Eng Data. 2004;49:453-461. https://doi.org/10.1021/je034102r
29. Chiappe C, Pieraccini D. ionic liquids: Solvent properties and organic reactivity. J Phys Org Chem.2005;18:275-297. https://doi.org/10.1002/poc.863
30. Mutelet F, Butet F, Jaubert JN. Application of inverse gas chromatography and regular solution theory for characterization of ionic liquids. Ind Eng Chem Res. 2005;44:4120-4127. https://doi.org/10.1021/ie048806I

31. Lagrost C, Carrie D, Vaultier M et al. Reactivities of some electrogenerated organic cation radicals in room-temperature ionic liquids: Toward an alternative to volatile organic solvents. J Phys Chem A. 2003;107:745-752. https://doi.org/10.1021/jp026907w
32. Guo L, Qi C, Zheng X et al. Toward understanding the adsorption mechanism of large size organic corrosion inhibitors on a Fe(110) surface using the DFTB method. RSC Adv. 2017;7:29042-29050. https://doi.org/10.1039/C7RA04120A
33. Mehmeti V, Berisha AR. Corrosion Study of Mild Steel in Aqueous Sulfuric Acid Solution Using 4-Methyl-4H-1,2,4-Triazole-3-Thiol and 2- Mercaptonicotinic Acid-An Experimental and Theoretical Study. Front Chem. 2017;5:61. https://doi.org/10.3389/fchem.2017.00061
34. Kolle P, Dronskowski R. Synthesis, crystal structures and electrical conductivities of the ionic liquid compounds butyl dimethylimidazoliumtetrafluoroborate, hexafluoroborate and hexafluoroantimonate. Eur J Inorg Chem. 2004;2313-2320. https://doi.org/10.1002/ejic.200300940
35. Berisha A, Podvorica FI, Vataj R et al. Corrosion Inhibition Study of Mild Steel in an Aqueous Hydrochloric Acid Solution Using Brilliant Cresyl Blue a Combined Experimental and Monte Carlo Study. Port Electrochim Acta. 2021;39:393-401. https://doi.org/10.4152/pea.2021390601
36. Suleiman RK, Saleh A, Charles O et al. Corrosion and fouling protection performance of biocide-embedded hybrid organosiloxane coatings on mild steel in a saline medium. Surf Coat Technol. 2017;324:526-35. https://dx.doi.org/10.1016/j.surfcoat.2017.06.028
37. Welton T. Room-temperature ionic liquids: Solvents for synthesis and catalysis. Chem Rev. 1999;99:2071-2084. https://doi.org/10.1021/cr980032t
38. Wilkes JSJ, Levisky A, Wilson RA et al. Dialkylimidazolium chloroaluminate melts, a new class of room-temperature ionic liquids for electrochemistry, spectroscopy and synthesis. Inorg Chem. 1982;21:1263-1264. https://doi.org/10.1021/ic00133a078)
39. Fannin AA, Floreani DA, King LA et al. Properties of 1,3-dialkylimidazolium chloride aluminium chloride ionic liquids. Part 2. J Phys Chem. 1984;88:2614-2627. https://doi.org/10.1021/j150656a038